Exceptional points in transistor-metamaterial-inspired transmission lines

David E. Fernandes[1,*] Sylvain Lannebère[2,†] Tiago A. Morgado[2,‡] and Mário G. Silveirinha[1,§]

[1]*University of Lisbon, Instituto Superior Técnico and Instituto de Telecomunicações, Avenida Rovisco Pais, 1, 1049-001 Lisboa, Portugal*

[2]*Instituto de Telecomunicações and Department of Electrical Engineering, University of Coimbra, 3030-290 Coimbra, Portugal*

Motivated by our recent findings in [Phys. Rev. Lett. 128, 013902, 2022], which introduced a new class of electromagnetic bulk materials whose response is similar to conventional semiconductor transistors, here we propose a one-dimensional (1D) version of such materials based on transmission lines coupled with FET isolators. We demonstrate that the response of this 1D system is nonreciprocal and non-Hermitian, analogous to the idealized transistor-metamaterial, and is also characterized by a broken time-reversal symmetry. We analyze the wave propagation in the system and find that the interaction between the eigenmodes can either lead to gain or loss, depending on the propagation distance. Furthermore, it is also shown that the system may be operated at an exceptional point, wherein the response becomes singular, and the power gain is maximized. Finally, we demonstrate that the exceptional point coincides with the point of operation of typical microwave amplifiers, such as the distributed amplifier.

I. INTRODUCTION

Hermiticity is a feature of physical systems related to energy conservation. In a Hermitian system, the dynamics of the state vector are conservative and governed by unitary (linear) operations [1]. Hermitian systems have a real-valued energy spectrum with their eigenvectors forming an orthogonal basis [1,2]. In the case of electrodynamics, a Hermitian material response requires that the permittivity and permeability tensors satisfy $\bar{\varepsilon} = \bar{\varepsilon}^{\dagger}$ and $\bar{\mu} = \bar{\mu}^{\dagger}$, with the dagger symbolizing the conjugate transpose (commonly referred to as the Hermitian conjugate). In recent years, there has been considerable interest in deliberately designing systems that deviate from Hermitian principles to achieve unprecedented control over light, enabling phenomena such as unidirectional propagation, enhanced sensitivity at exceptional points, and tailored dispersion relations [3–10]. Achieving this non-Hermitian response involves a variety of strategies, such as harnessing parity-time ($\mathcal{PT}$) symmetry [11–13], incorporating active electronic elements into system design [14–16] or components with optical gain [17].

Furthermore, in Ref. [18], we recently proposed a mechanism to obtain a strong nonreciprocal and non-Hermitian

response based on the interaction between a static electric bias and material nonlinearities, analogous to the response of standard metal-oxide-semiconductor field-effect transistors (MOSFETs). In Refs. [18–20], it was demonstrated that the response of this MOSFET metamaterial (MOSFET-MTM) can either exhibit optical gain or dissipation depending on the relative phase of the electric field components inside the material. Such metamaterial may be useful to obtain robust electromagnetic isolation and amplification.

In this work, we investigate a 1D implementation of the MOSFET-MTM based on transmission lines coupled with FET isolators. We theoretically show that the response of the structure is nonreciprocal, non-Hermitian, and is characterized by a broken time-reversal symmetry. We demonstrate that the interaction between the system eigenmodes can enable regimes with gain and loss, depending on the propagation distance.

An important feature of non-Hermitian systems is that their eigenstates are generally nonorthogonal and that their energy spectrum is complex-valued. This attribute endows these systems with unique characteristics, among which the emergence of exceptional points stands out [21–23]. At an exceptional point, the non-Hermitian operator or matrix becomes defective, leading to a singularity in which two or more eigenvalues (and the associated eigenvectors) coalesce and become degenerate [21,23]. Exceptional points have received significant attention for the unparalleled opportunities that they offer in enhancing sensing

---

*Contact author: dfernandes@co.it.pt
†Contact author: sylvain.lannebere@co.it.pt
‡Contact author: tiago.morgado@co.it.pt
§Contact author: mario.silveirinha@co.it.pt

024003-1

capabilities [24–29]. Exceptional points have also been studied in the context of chiral transport and topological phenomena [30–36], unidirectional invisibility [37–40], formation of bulk Fermi arcs [41], and unusual quantum criticality [42–48]. It is important to mention that degeneracies in the eigenvalues may also be observed in Hermitian systems [22,49]; however, the corresponding eigenvectors can still form an orthogonal basis. Here, based on the MOSFET metamaterial concept, we propose a method to operate two asymmetrically coupled transmission lines at an exceptional point. We show that at the exceptional point, the response becomes singular and the system behaves as an amplifier whose gain increases with the square of the number of transistors, similar to the well-known distributed amplifier [50–53].

This paper is organized as follows. In Sec. II, we briefly describe the main characteristics and wave propagation properties of the MOSFET-MTM. In Sec. III, we propose a possible implementation of the MOSFET-MTM based on capacitively coupled transmission lines. We analyze the wave propagation within the structure, demonstrating the feasibility of operating it at an exceptional point. The operation at the degeneracy point is marked by a substantial power gain. Finally, in Sec. IV, the conclusions are drawn. The time dependence of the fields is assumed of the type $e^{-i\omega t}$, where ω is the oscillation frequency.

II. MOSFET METAMATERIAL

The MOSFET metamaterial (MOSFET-MTM) is an idealized material that exploits the interaction between an electric static bias and material nonlinearities, drawing inspiration from the response of standard MOSFETs [18]. In the MOSFET-MTM, the relation between the polarization vector **P** and the electric field **E** is $\mathbf{P} = \varepsilon_0 \bar{\chi}(\mathbf{E}) \cdot \mathbf{E}$, with the susceptibility tensor given by

$$\overline{\chi}(\mathbf{E}) = \begin{pmatrix} \chi_{xx}(E_z) & 0 & 0 \\ 0 & \chi_{yy} & 0 \\ 0 & 0 & \chi_{zz} \end{pmatrix}. \quad (1)$$

The susceptibility tensor is a nonlinear function of the electric field, as the component $\chi_{xx}(E_z)$ depends on the electric field along the z-direction, E_z. It was shown in Ref. [18] that when this material is biased by a static electric field $\mathbf{E}_0$ in the x-z plane ($\mathbf{E}_0 = E_{x0}\hat{\mathbf{x}} + E_{z0}\hat{\mathbf{z}}$), the effective linearized response of the material, i.e., the response of the material for small variations of the electric field around the biasing point $\delta\mathbf{P} = \varepsilon_0 \bar{\chi}_{\text{lin}}(\mathbf{E}) \cdot \delta\mathbf{E}$, with $\mathbf{E} = \mathbf{E}_0 + \delta\mathbf{E}$ and $\delta\mathbf{E} \ll \mathbf{E}_0$, may be described by the following linearized susceptibility tensor:

$$\bar{\chi}_{\text{lin}} = \begin{pmatrix} \chi_{xx}(E_{z0}) & 0 & \partial_{E_z}\chi_{xx}(E_{z0})E_{x0} \\ 0 & \chi_{yy} & 0 \\ 0 & 0 & \chi_{zz} \end{pmatrix}. \quad (2)$$

As the displacement vector **D** relates the fields as $\mathbf{D} = \varepsilon_0\mathbf{E} + \mathbf{P}$, it follows that the relative effective linearized permittivity of the MOSFET-MTM may be written as [18]

$$\bar{\varepsilon} = \mathbf{1} + \bar{\chi}_{\text{lin}} = \begin{pmatrix} \varepsilon_{xx} & 0 & \varepsilon_{xz} \\ 0 & \varepsilon_{yy} & 0 \\ 0 & 0 & \varepsilon_{zz} \end{pmatrix}. \quad (3)$$

As $\bar{\varepsilon} \neq \bar{\varepsilon}^\dagger$, the response of the MOSFET-MTM is non-Hermitian. Furthermore, since $\bar{\varepsilon} \neq \bar{\varepsilon}^T$, the material is also nonreciprocal.

To analyze the consequences of this type of metamaterial response, let us consider the plane wave propagation problem. Since we are only considering the linearized response of the MOSFET-MTM, for notational simplicity, we replace $\delta\mathbf{E} \to \mathbf{E}$. The fields in the material can be determined from the Maxwell equations, i.e.,

$$\nabla \times \mathbf{E} = i\omega\mu_0\mathbf{H}, \quad (4a)$$

$$\nabla \times \mathbf{H} = -i\omega\varepsilon_0\bar{\varepsilon} \cdot \mathbf{E}. \quad (4b)$$

For propagation along the y-direction ($\nabla = \partial_y\hat{\mathbf{y}}$), Eqs. (4a) and (4b) may be rewritten in an expanded form as follows:

$$i\partial_y E_x = \omega\mu_0 H_z, \quad (5a)$$

$$i\partial_y E_z = -\omega\mu_0 H_x,$$
$$i\partial_y H_x = -\omega\varepsilon_0\varepsilon_{zz}E_z, \quad (5b)$$
$$i\partial_y H_z = \omega\varepsilon_0(\varepsilon_{xx}E_x + \varepsilon_{xz}E_z).$$

By defining a state vector $\mathbf{f} = \left(E_x, E_z, -H_z, H_x\right)^T$, the Maxwell equations can be written in a compact matrix form as $i\partial_y\mathbf{f} = \mathbf{M} \cdot \mathbf{f}$, with **M** equal to

$$\mathbf{M} = -\omega \begin{pmatrix} 0 & 0 & \mu_0 & 0 \\ 0 & 0 & 0 & \mu_0 \\ \varepsilon_0\varepsilon_{xx} & \varepsilon_0\varepsilon_{xz} & 0 & 0 \\ 0 & \varepsilon_0\varepsilon_{zz} & 0 & 0 \end{pmatrix}. \quad (6)$$

Assuming $\mathbf{k} = k_y\hat{\mathbf{y}}$, so that $\partial_y = ik_y$, the eigenmodes in the bulk material can be determined from the nontrivial solutions of the characteristic equation, i.e.,

$$\det\left(\mathbf{M} + k_y\mathbf{1}_{4\times4}\right)$$
$$= \left(k_y^2 - \left(\frac{\omega}{c}\right)^2\varepsilon_{xx}\right)\left(k_y^2 - \left(\frac{\omega}{c}\right)^2\varepsilon_{zz}\right) = 0.$$

There are two eigenmodes (two solutions for k_y^2) that can be identified as ordinary and extraordinary waves [18]. Due to the non-Hermitian response, the corresponding eigenvectors are not orthogonal. As described in Ref. [18], such a property can give rise to unique wave phenomena,

such as regimes with optical gain or dissipation that depend on the relative phase of the (position-dependent) electric field components in the material. In particular, the metamaterial can serve as a building block to realize optical isolators and other nonreciprocal and active devices [18].

III. TRANSMISSION-LINE MODEL

In this section, we suggest a straightforward approach for implementing MOSFET-MTM devices in the microwave range based on transmission-line (1D) technology and FETs. Furthermore, we study the unique wave phenomena that arise from the MOSFET-MTM response.

The idea is to exploit a parallelism between Maxwell's equations in a MOSFET-MTM [Eqs. (5a) and (5b)] and the transmission-line equations [53]. In a coupled transmission-line configuration, such as the one shown in Fig. 1(a), the wave equations for propagation along the y-direction read as

$$\partial_y V_1 = i\omega L_{11} I_1, \tag{7a}$$

$$\partial_y I_1 = i\omega(C_{11}V_1 + C_{12}V_2), \tag{7b}$$

$$\partial_y V_2 = i\omega L_{22} I_2, \tag{7c}$$

$$\partial_y I_2 = i\omega(C_{21}V_1 + C_{22}V_2). \tag{7d}$$

Here, C_{21} and C_{12} represent the mutual capacitances per unit of length, which describe the coupling between the two lines, and C_{11} and C_{22} are the capacitances per unit of length of each line alone. The inductances per unit of length of each line are L_{11} and L_{22}. We neglect the inductive coupling between the lines, so that $L_{12} = L_{21} = 0$, as well as the dissipation effects in the materials.

It is easy to check that the electromagnetic fields and the material parameters can be mapped into equivalent transmission-line voltages/currents and inductances/capacitances, respectively, by using the following transformation rules:

$$E_x \rightarrow V_1, \quad E_z \rightarrow V_2, \tag{8a}$$
$$-H_z \rightarrow I_1, \quad H_x \rightarrow I_2,$$

$$\mu_0 \rightarrow L_{11}, L_{22},$$
$$\varepsilon_0\varepsilon_{xx} \rightarrow C_{11}, \quad \varepsilon_0\varepsilon_{zz} \rightarrow C_{22}, \quad \varepsilon_0\varepsilon_{xz} \rightarrow C_{12}, \tag{8b}$$
$$\varepsilon_0\varepsilon_{zx} \rightarrow C_{21}.$$

Hence, in order to mimic the response of the MOSFET-MTM, the coupled lines are required to have $C_{12} \neq 0$ and $C_{21} = 0$. This type of asymmetric coupling causes the response of line 1 to be influenced by the waves propagating in line 2, whereas line 2 is completely isolated from line 1. In practice, this arrangement can be realized by employing two microstrip lines periodically loaded with FET isolators, as illustrated in Fig. 1(b). The transistors are three-port devices that consist of the drain, gate, and source. We adopt a common-source configuration so that the source is connected to the ground plane of the microstrip lines. The gate is connected to line 2 (gate line) and the drain is connected to line 1 (drain line). The response of the FET is modeled through an admittance matrix

$$\mathbf{Y}_F = \begin{pmatrix} Y_{F,11} & Y_{F,12} \\ Y_{F,21} & Y_{F,22} \end{pmatrix},$$

which relates the currents and voltages at the two ports. The admittance matrix is determined from the small signal equivalent circuit of the FET, which results from a linearization of the response around an operation point [53]. A similar linearization procedure is employed in the analysis of the MOSFET-MTM [18]. Figure 2 depicts the small signal equivalent circuit of the FETs under a common-source configuration [53]. The elements of the admittance
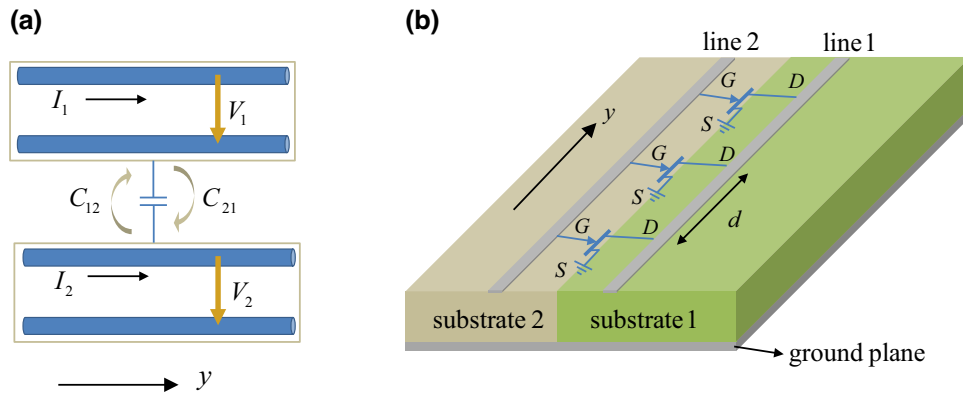

FIG. 1. (a) Two sets of transmission lines are capacitively coupled through mutual capacitances C_{12} and C_{21}. (b) Transmission line implementation of the MOSFET-MTM: two microstrip transmission lines oriented along the y-direction are periodically loaded with FET isolators (with spatial period d). We use a common-source configuration wherein the source is connected to the ground plane, the drain is connected to line 1, and the gate is connected to line 2.
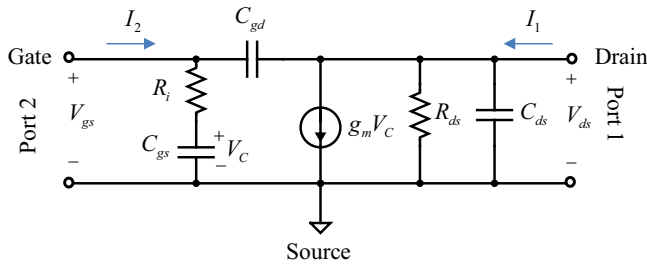
FIG. 2.   Small signal equivalent circuit for a microwave FET in the common-source configuration: C_{gd} is the gate-to-drain capacitance, C_{gs} is gate-to-source capacitance, C_{ds} is drain-to-source capacitance, g_m is the transconductance of the FET, R_i is the series gate resistance, and R_{ds} is the drain-to-source resistance. We take port 1 as the drain of the FET and port 2 as the gate.

matrix are defined as $Y_{F,mn} = \left. \dfrac{I_m}{V_n} \right|_{V_k=0 \text{ for } k \neq n}$, with $m, n =$ 1, 2 identifying the ports 1 and 2 of the FET.

A straightforward analysis shows that the admittance matrix of the FET equivalent circuit (Fig. 2) is given by the following:

$$\mathbf{Y}_F = \begin{pmatrix} \dfrac{1}{R_{ds}} - i\omega(C_{ds} + C_{gd}) & \dfrac{g_m}{(-i\omega C_{gs}R_i + 1)} + i\omega C_{gd} \\[2ex] i\omega C_{gd} & \left(R_i - \dfrac{1}{i\omega C_{gs}}\right)^{-1} - i\omega C_{gd} \end{pmatrix},$$ (9)

where C_{gd}, C_{gs}, and C_{ds} are the gate-to-drain, gate-to-source, and drain-to-source capacitances, respectively. Moreover, g_m is the transconductance of the FET, R_i is the series gate resistance, and R_{ds} is the drain-to-source resistance. The gate-to-drain capacitance C_{gd} is usually small and can often be ignored [53]. In the following, we neglect C_{gd} except when explicitly stated otherwise. In this case, $Y_{F,21} \approx 0$, so that the gate becomes effectively isolated from the drain but not the other way around.

Ideally, it is desired that (i) $\omega C_{gs} R_i \ll 1$ and (ii) $\omega C_{ds} R_{ds} \gg 1$ to avoid insertion losses. While the first condition relates to the intrinsic loss of the FET (ideally, R_i should be as small as possible), the second condition can be met by setting the point of operation of the FET in the saturation regime [53] so that the drain-source current $I_{ds} = V_{ds}/R_{ds}$ is weakly sensitive to variations in the drain-source voltage $V_{ds} = V_1$. This is equivalent to having a very large R_{ds}.

For sufficiently long wavelengths, so that $\lambda \gg d$, it is possible to homogenize the periodic FET loading and model the system of Fig. 1 as a uniform "medium." The FET loading contributes to the capacitance per unit of length of the homogenized line. The additional capacitance per unit of length is given by $\mathbf{Y}_F/(-i\omega d)$. Thus, the transistor effect is spread uniformly along the line. Hence,

the effective capacitance matrix $\mathbf{C}_{ef}$ of the homogenized system may be written as

$$\mathbf{C}_{ef} = \begin{pmatrix} C_{11} & 0 \\ 0 & C_{22} \end{pmatrix} + \frac{\mathbf{Y}_F}{(-i\omega d)},$$ (10)

whereas the effective inductance matrix is given by

$$\mathbf{L}_{ef} = \begin{pmatrix} L_{11} & 0 \\ 0 & L_{22} \end{pmatrix}.$$ (11)

The continuous model is expected to be accurate provided that the distance between the transistors is much smaller than the operation wavelength, the so-called metamaterial regime. Later, we shall confirm the validity of this approach. In the ideal case of a nondissipative FET operated in the saturation regime ($R_i \approx 0$ and $R_{ds} \approx \infty$), the effective capacitance reduces to

$$\mathbf{C}_{ef} \approx \begin{pmatrix} C_{11} + \dfrac{C_{ds}}{d} & \dfrac{g_m}{-i\omega d} \\[2ex] 0 & C_{22} + \dfrac{C_{gs}}{d} \end{pmatrix}.$$ (12)

As seen, it has exactly the same structure as the permittivity of the 3D metamaterial [compare with Eq. (3)]. There is, however, a key difference: here the capacitance $C_{ef,12}$ is purely imaginary, whereas the corresponding permittivity component ε_{xz} in the MOSFET-MTM was assumed real-valued in Ref. [18]. In particular, different from Ref. [18], here, the system response, albeit non-Hermitian, is characterized by a broken time-reversal symmetry [$\mathbf{C}_{ef}(\omega) \neq \mathbf{C}_{ef}(\omega^*)^*$]. Note that the response is also nonreciprocal because $\mathbf{C}_{ef}$ does not have transpose symmetry.

A. Transmission-line modes

The wave propagation in the homogenized lines is described by the linear system (7), with the effective capacitive and inductive elements determined by Eqs. (10) and (11), respectively. We can write Eqs. (7a)–(7d) in a compact form as $i\partial_y \mathbf{f} = \mathbf{M} \cdot \mathbf{f}$, with the matrix $\mathbf{M}$ given by

$$\mathbf{M} = -\omega \begin{pmatrix} 0 & 0 & L_{11} & 0 \\ 0 & 0 & 0 & L_{22} \\ C_{ef,11} & C_{ef,12} & 0 & 0 \\ C_{ef,21} & C_{ef,22} & 0 & 0 \end{pmatrix}.$$ (13)

The 4-component state vector is defined by $\mathbf{f} = (\mathbf{V}, \mathbf{I})^T$, with $\mathbf{V} = (V_1, V_2)^T$ and $\mathbf{I} = (I_1, I_2)^T$. Using these notations, we can obtain the traveling wave type solutions (bulk eigenmodes with a spatial variation along y of the form $e^{i\beta y}$) from the eigenvalues and eigenvectors of matrix $\mathbf{M}$, similar to the MOSFET-MTM. The system supports two

eigenwaves propagating along the $+y$-direction and two eigenwaves propagating in the opposite direction.

For simplicity, in the following, we focus the analysis on the particular case wherein the capacitance matrix is given by Eq. (12), so that $C_{ef,21} = 0$. In such a scenario, line 2 is perfectly isolated from line 1. Consequently, the system supports an "ordinary" wave characterized by a propagation constant $\beta_\mathrm{o} = \omega\sqrt{L_{11}C_{ef,11}}$ and eigenvector

$$\mathbf{f}_\mathrm{o} = \left(\mathbf{V}_\mathrm{o}, \mathbf{I}_\mathrm{o}\right)^T = A_\mathrm{o}\left(\sqrt{\frac{L_{11}}{C_{ef,11}}}, 0, 1, 0\right)^T e^{i\beta_\mathrm{o}y}. \quad (14)$$

Note that this wave is insensitive to cross-capacitive coupling: the energy propagates exclusively in line 1 (drain line). In addition, it also supports an extraordinary wave with propagation constant $\beta_\mathrm{e} = \omega\sqrt{L_{22}C_{ef,22}}$ and eigenvector

$$\mathbf{f}_\mathrm{e} = \left(\mathbf{V}_\mathrm{e}, \mathbf{I}_\mathrm{e}\right)^T$$
$$= A_\mathrm{e}\left(\sqrt{\frac{L_{22}}{C_{ef,22}}}\frac{C_{ef,12}L_{11}}{C_{ef,22}L_{22} - C_{ef,11}L_{11}},\right.$$
$$\left.\sqrt{\frac{L_{22}}{C_{ef,22}}}, \frac{C_{ef,12}L_{11}}{C_{ef,22}L_{22} - C_{ef,11}L_{11}}, 1\right)^T e^{i\beta_\mathrm{e}y}. \quad (15)$$

This mode can be understood as a wave propagating in line 2 (gate line), which is coupled to line 1 (drain line) through the unidirectional FETs. The coupling factor $C_{ef,12}$ is determined by the transconductance of the FET isolators. In the above, A_o and A_e are the complex amplitudes of the ordinary and extraordinary waves, respectively. Note that the modes described above propagate along the $+y$-direction. The modes propagating in the opposite direction are characterized by the same propagation constants β_o and β_e.

A generic solution of the system $i\partial_y\mathbf{f} = \mathbf{M}\cdot\mathbf{f}$ is a superposition of ordinary and extraordinary waves propagating in the coupled lines. In particular, a wave propagating along the $+y$-direction is of the form $\mathbf{f} = \mathbf{f}_\mathrm{o} + \mathbf{f}_e = (\mathbf{V}_\mathrm{o} + \mathbf{V}_\mathrm{e}, \mathbf{I}_\mathrm{o} + \mathbf{I}_\mathrm{e})^T$. Taking into account that the total power flowing in the lines is given by $P(y) = (1/2)\mathrm{Re}\{\mathbf{V}\cdot\mathbf{I}^*\}$, one readily finds that

$$P(y) = \frac{1}{2}\mathrm{Re}\{\mathbf{V}_\mathrm{o}\cdot\mathbf{I}_\mathrm{o}^*\} + \frac{1}{2}\mathrm{Re}\{\mathbf{V}_\mathrm{e}\cdot\mathbf{I}_\mathrm{e}^*\}$$
$$+ \frac{1}{2}\mathrm{Re}\{\mathbf{V}_\mathrm{e}\cdot\mathbf{I}_\mathrm{o}^* + \mathbf{V}_\mathrm{o}\cdot\mathbf{I}_\mathrm{e}^*\}. \quad (16)$$

Evidently, we can identify $P_\mathrm{o} = (1/2)\mathrm{Re}\{\mathbf{V}_\mathrm{o}\cdot\mathbf{I}_\mathrm{o}^*\}$ and $P_e = (1/2)\mathrm{Re}\{\mathbf{V}_\mathrm{e}\cdot\mathbf{I}_\mathrm{e}^*\}$ as the contributions of the ordinary and extraordinary waves alone, while the remaining part $P_\mathrm{cr} = (1/2)\mathrm{Re}\{\mathbf{V}_\mathrm{e}\cdot\mathbf{I}_\mathrm{o}^* + \mathbf{V}_\mathrm{o}\cdot\mathbf{I}_\mathrm{e}^*\}$ is an interference term

resulting from the interaction between the two waves. Since this interference term depends on the relative phase between the propagation constants of the modes, it can give rise to a power oscillation when the waves propagate simultaneously along the line. To illustrate the "power beating" characteristic, we assume that the structure represented in Fig. 1 is excited at the input ($y = 0$) of the gate line (line 2) and that the drain line (line 1) is short-circuited at the input. Both lines are terminated with matched loads to avoid reflections. For a superposition of the ordinary and extraordinary modes [Eqs. (14) and (15)], it is simple to show that $V_1(y = 0) = 0$ requires that the complex amplitudes of the waves satisfy

$$A_o = -A_e\sqrt{\frac{C_{ef,11}}{L_{11}}}\sqrt{\frac{L_{22}}{C_{ef,22}}}\frac{C_{ef,12}L_{11}}{C_{ef,22}L_{22} - C_{ef,11}L_{11}}. \quad (17)$$

We consider that the unloaded lines are identical. Moreover, the lines have characteristic impedance $Z_{01} = Z_{02} = Z_0 = 50\ \Omega$ and effective permittivity $\varepsilon_{ef,2} = \varepsilon_{ef,1} = \varepsilon_{ef} = 1.7$. The effective permittivity represents the permittivity of an equivalent uniform medium that models the combined effect of the air and dielectric regions in the microstrip line [53]. Hence, the per unit of length capacitances and inductances of the uncoupled lines are $C_{ii} = 1/(Z_0v_p)$ and $L_{ii} = Z_0/v_p$, respectively, with $v_p = c/\sqrt{\varepsilon_{ef}}$ the phase velocity in the lines. The lines are coupled through FET isolators characterized by [53]: $C_{gs} = 0.3$ pF, $C_{ds} = 0.12$ pF, and $g_m = 40$ mS. Moreover, we assume that the distance between adjacent transistors (spatial period) is $d = 5$ mm.

Figure 3(a) shows the spatial distribution of the power transported in the system at the fixed frequency of operation $\omega/(2\pi) = 5$ GHz. As seen, the power oscillates periodically with the propagation distance, similar to the MOSFET-MTM [18]. In the sections where the power increases [shaded brown regions in Fig. 3(a)], the transistors inject energy into the system, yielding a substantial rise in transported power that can surpass more than 180 times the input power. Conversely, within the dissipative regions [shaded green areas in Fig. 3(a)], the FET isolators extract energy from the lines, resulting in a reduction of transported power. It is important to mention that despite no dissipative elements being explicitly considered in this example, the response of the FET can lead to absorption. Indeed, even in the ideal case, when $R_i = 0$ and $R_{ds} = \infty$, the transistors can extract energy from the ac signal through the current source associated with the transconductance gain, resulting in a dissipative response. Thus, different from more conventional gain systems, the MOSFET-type response can either be active or dissipative, depending on the relative phase between the voltages at the gate and drain lines.

We have also calculated the power transported by the two lines separately, given by $P_i(y) = (1/2)\mathrm{Re}\{\mathbf{V}_i\cdot\mathbf{I}_i^*\}$,
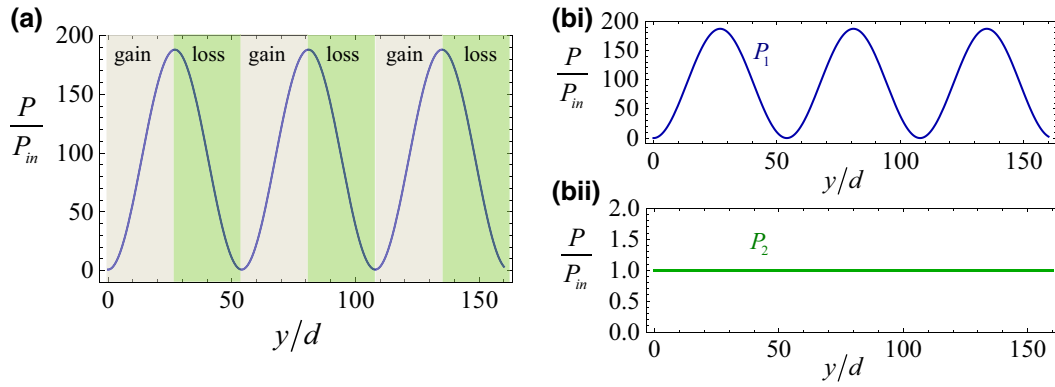
FIG. 3. (a) Normalized power transported by the coupled lines as a function of the propagation distance normalized to the spacing $d = 5$ mm between adjacent FETs for the frequency of operation $\omega/(2\pi) = 5$ GHz. The microstrip lines have the same characteristic impedance $Z_{01} = Z_{02} = Z_0 = 50\ \Omega$ and effective permittivity $\varepsilon_{ef,2} = \varepsilon_{ef,1} = \varepsilon_{ef} = 1.7$. The FET isolators have $R_i = 0$, $R_{ds} = \infty$, $C_{gs} = 0.3$ pF, $C_{ds} = 0.12$ pF, $g_m = 40$ mS, and $C_{gd} = 0$. The regions shaded in green correspond to dissipative regions, whereas the light-brown shaded regions correspond to gain regions. (b) Similar to (a) but showing the normalized power transported by the (i) drain line (blue curve) and (ii) gate line (green curve).

for $i = 1, 2$. The results are depicted in Fig. 3(b) and show that while the power transported in the gate line remains constant and equal to $P_2 = P_{in}$ (green curve), the power transported in the drain line (blue curve) oscillates. This feature stems from the unidirectional properties of the transistors. The gate line is isolated from the drain line, whereas the drain line is coupled to the gate line. Thus, the power transported in the drain line results from the interference of two waves, leading to power oscillations. Similar to standard transistor-based devices, the physical origin behind the power oscillations is the energy supplied by the dc generator that biases the transistors, which can be positive or negative. The type of response, active or dissipative, depends on the relative phase of the current and voltage at the transconductance element. The latter describes how the energy is transferred from the dc part of the circuit to the ac part of the circuit, through the nonlinear response of the transistor.

Up to this point, the wave propagation was described using the continuum model. However, it is important to consider the intrinsic granularity of the system by incorporating the periodic loading of transistors along the lines. In this case, it is convenient to regard the structure as an arrangement of a finite number of unit cells. We suppose that the transistor is placed in the middle of a unit cell comprising two microstrip line sections with length $d/2$. Then, the state vector at the output of the unit cell is related to the state vector at the input as $\mathbf{f}(y = d) = \left(e^{-i\mathbf{M}_0(d/2)} \cdot \mathbf{T} \cdot e^{-i\mathbf{M}_0(d/2)}\right) \cdot \mathbf{f}(y = 0)$, where $\mathbf{M}_0$ is the material matrix of the bare transmission lines given by

$$\mathbf{M}_0 = -\omega \begin{pmatrix} 0 & 0 & L_{11} & 0 \\ 0 & 0 & 0 & L_{22} \\ C_{11} & 0 & 0 & 0 \\ 0 & C_{22} & 0 & 0 \end{pmatrix}, \quad (18)$$

and $\mathbf{T}$ is the transfer matrix of the FET that is written as:

$$\mathbf{T} = \begin{pmatrix} 1 & 0 & 0 & 0 \\ 0 & 1 & 0 & 0 \\ -Y_{11} & -Y_{12} & 1 & 0 \\ -Y_{21} & -Y_{22} & 0 & 1 \end{pmatrix}, \quad (19)$$

which depends on the admittance matrix given in Eq. (9). For a finite structure with N cells, one can relate the state vector at the input and the output of the system as $\mathbf{f}(y = Nd) = \left(e^{-i\mathbf{M}_0(d/2)} \cdot \mathbf{T} \cdot e^{-i\mathbf{M}_0(d/2)}\right)^N \cdot \mathbf{f}(y = 0)$.

Next, we compare the continuum model results with the exact solution that takes into account the discrete nature of the structure. As before, it is supposed that $V_1(y = 0) = 0$. Figure 4(a) shows the power distribution in the lines for the same configuration as in Fig. 3. In the discrete model, we only show the normalized power calculated at the input of each unit cell (consecutive discrete nodes are spaced by a distance d). The results of Fig. 4(a) show a remarkable agreement between the continuous and discrete models, indicating that the continuous model describes the wave propagation in the system very accurately, particularly for short propagation distances ($y/d < 50$).

We also studied the response of the system when the frequency of operation is increased. Figure 4(b) depicts the results of the continuous and discrete models for a frequency of operation $\omega/(2\pi) = 7.5$ GHz. As seen, compared with the configuration studied in Fig. 4(a), the peak amplitude of the power transported in the lines decreases to about half, and the spatial period of the oscillations also decreases. The agreement between the two models is less apparent in Fig. 4(b). The discrepancy between the results of the continuous and the exact solution is an inherent limitation of the continuous model, which is only applicable in the long wavelength regime where $\omega d/c \ll 1$. In Fig. 4(b), the normalized frequency ($\omega d/c \approx 0.79$) is higher than in
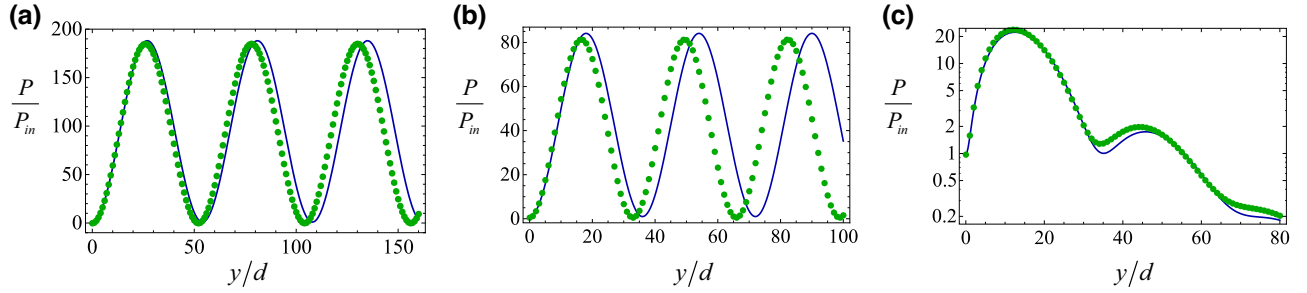
FIG. 4. (a) Normalized (total) power transported by the coupled lines as a function of the propagation distance for the same coupled transmission-line configuration studied in Fig. 3. (b) Similar to (a) but for the operation frequency $\omega/(2\pi) = 7.5$ GHz. (c) Similar to (b) but considering the dissipative elements of the transistor model. In all the plots, the solid curves represent the continuous model results and the symbols correspond to the discrete model results.

Fig. 4(a) ($\omega d/c \approx 0.52$), which contributes to the weaker agreement between models.

Additionally, we investigated the impact of dissipation in the FETs on the overall response of the coupled lines. The dissipation in the FET isolators is considered by taking $R_i = 7\ \Omega$ and $R_{ds} = 400\ \Omega$ [53]. The corresponding power distribution in the lines calculated with the continuous and discrete models is shown in Fig. 4(c). Interestingly, it is observed that the power in the system can experience oscillations even in the presence of the dissipative elements of the transistor model. However, the maximum gain undergoes a significant reduction, approximately fourfold, and the power beating is markedly dampened, becoming indistinct for $y/d > 80$.

B. Exceptional points

As discussed in the previous section, the response of the coupled lines is non-Hermitian and, thereby, the bulk eigenstates are nonorthogonal. Importantly, the response of a non-Hermitian system can become singular when two or more eigenstates degenerate and coalesce. This is called an exceptional point. It is easy to check in our system that such a behavior ($\mathbf{f}_e \sim \mathbf{f}_o$) emerges in the continuous model when $L_{22}C_{ef,22} = L_{11}C_{ef,11}$. In such a scenario, both eigenmodes share an identical propagation constant, i.e., $\beta_o = \beta_e$, and the same field structure. At the exceptional point, the general solution of $i\partial_y \mathbf{f} = \mathbf{M} \cdot \mathbf{f}$ is not generated by complex exponentials only but rather by a combination of complex exponentials and polynomials of y, which is written as

$$V_1 = A_1^+ e^{i\beta_o y} + A_1^- e^{-i\beta_o y}$$
$$+ \frac{C_{12,ef}}{2C_{11,ef}}i\beta_o y\left[B_2^+ e^{i\beta_o y} - B_2^- e^{-i\beta_o y}\right]\text{(drain line)},$$

$$\tag{20a}$$

$$V_2 = B_2^+ e^{i\beta_o y} + B_2^- e^{-i\beta_o y}\text{ (gate line)}. \tag{20b}$$

The currents can be found from the voltages using Eqs. (7a) and (7c). As seen, due to the term proportional to y, the voltage in the drain line can be arbitrarily large at the exceptional point and, hence, the peak gain is not constrained by the power beating oscillation. At the singular point, there is a resonant interaction between the ordinary and extraordinary waves due to the phase-matching condition $\beta_o d = \beta_e d$. Specifically, $\beta_o = \beta_e$ guarantees that the relative phase between the voltage and current at the transconductance elements does not change as the wave propagates. Thus, as the wave progresses along the line, it can continuously draw power from the dc bias, different from the situation where due to $\beta_o \neq \beta_e$ some of the power already propagating in the line can be returned to the dc bias.

In order to investigate the properties of the exceptional point in our system, we consider the same parameters and operation frequency ($\omega/(2\pi) = 5$ GHz) as in Fig. 3, except that now we suppose that the input line (line 2) is characterized by an effective permittivity $\varepsilon_{ef,2} = \alpha \varepsilon_{ef,1}$. As before, the line impedances are $Z_{01} = Z_{02} = Z_0 = 50\ \Omega$. In Fig. 5(a), we depict the propagation constants of the ordinary and extraordinary waves as a function of α. As seen, an exceptional point emerges for $\alpha = 0.699$ $\left(\varepsilon_{ef,2}^{\text{EP}} = 1.1883\right)$, which ensures that both propagation constants and the two eigenmodes coalesce.

At the exceptional point, the Bloch-wave type description breaks down as Eq. (15) becomes singular. The modes at the exceptional point have a polynomial nature, as shown in Eq. (20). Hence, by operating the system at an exceptional point, the power drawn from the dc supply is maximized. As the spacing between adjacent FETs is the same on both lines, the exceptional point $\beta_o = \beta_e$ occurs when the phase delay in the lines is identical. This is often referred to as the synchronization condition in the design of microwave amplifiers, such as the distributed amplifier [53]. From Eq. (20a), it is clear that when the lines are terminated with matched loads and for sufficiently large y, we
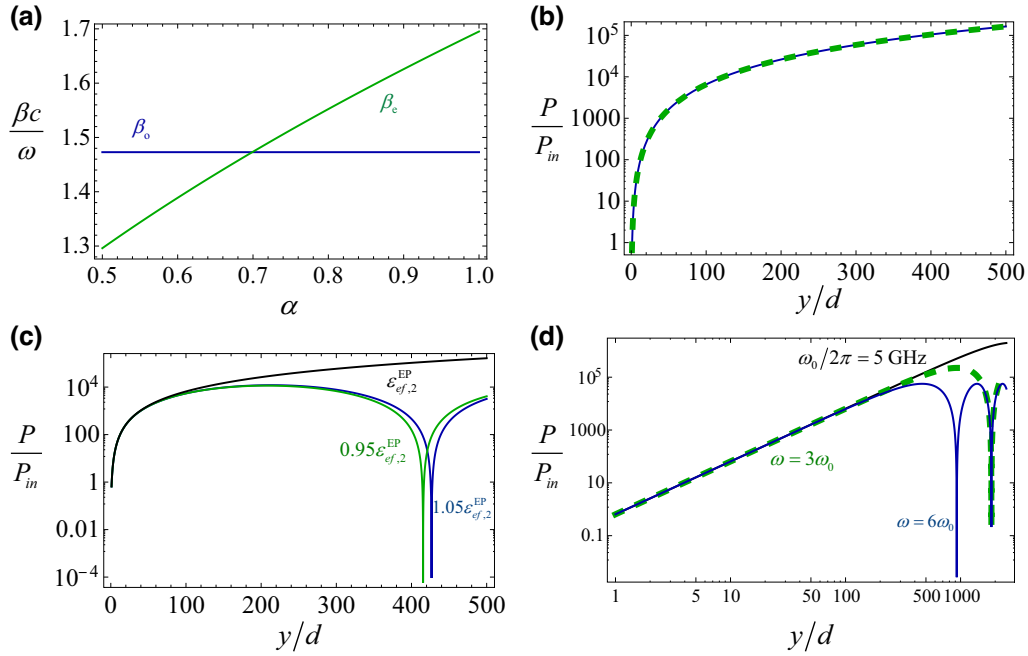
FIG. 5. (a) Normalized propagation constants of the ordinary (blue curve) and extraordinary (green curve) modes calculated as a function of $\alpha = \varepsilon_{ef,2}/\varepsilon_{ef,1}$ for the same structural parameters as in Fig. 3, except for the effective permittivity of line 2 $\left(\varepsilon_{ef,2}\right)$. (b) Power gain P/P_{in}, when the system is operated at the exceptional point $\left(\text{i.e., for } \varepsilon_{ef,2}^{\text{EP}} = 0.699\varepsilon_{ef,1}\right)$, for the structural parameters considered in (a). The solid blue line represents our theoretical (continuous model) results and the dashed line corresponds to the results predicted by Eq. (21). (c) Similar to (b) but calculated using $\varepsilon_{ef,2} = \varepsilon_{ef,2}^{\text{EP}}$ (black curve), $\varepsilon_{ef,2} = 1.05\varepsilon_{ef,2}^{\text{EP}}$ (blue curve), and $\varepsilon_{ef,2} = 0.95\varepsilon_{ef,2}^{\text{EP}}$ (green curve). (d) Similar to (b) but calculated at different frequencies $\omega/(2\pi) = \omega_0/(2\pi) = 5$ GHz (black solid curve), $\omega = 3\omega_0$ (green dashed curve), and $\omega = 6\omega_0$ (blue solid curve) with $C_{gd} = 0.01$ pF.

can take

$$V_1 \approx \frac{C_{12,ef}}{2C_{11,ef}} i\beta_{\text{o}} y B_2^+ e^{i\beta_{\text{o}} y} = \frac{C_{12,ef}}{2C_{11,ef}} i\beta_{\text{o}} y V_2.$$

Thus, the output (line 1) and input (line 2) powers are related as follows:

$$P_{\text{out}}/P_{\text{in}} \approx \left|\frac{C_{12,ef}}{2C_{11,ef}}\right|^2 |\beta_{\text{o}} y|^2 \frac{Z_g}{Z_d} = g_m^2 \frac{Z_g Z_d}{4}\left(\frac{y}{d}\right)^2$$

with $Z_g = \sqrt{L_{22}/C_{ef,22}}$ and $Z_d = \sqrt{L_{11}/C_{ef,11}}$. The power flowing in the line grows quadratically with the length of the line. The derived result can also be written as

$$G = \frac{P_{\text{out}}}{P_{\text{in}}} = \frac{g_m^2 Z_d Z_g N^2}{4}, \tag{21}$$

where N is the number of FETs in the structure. Curiously, the above formula is well-known in the design of distributed amplifiers [53], which thereby are operated at an exceptional point. The power gain grows quadratically with the number of FETs and also depends on the transconductance gain and the characteristic impedance of the effective lines. It is relevant to mention that, in most practical scenarios, the synchronization condition is enforced by

varying the distance between successive FET through the meandering of the transmission lines. Here, we consider lines with different dielectric substrates merely to simplify the analytical modeling.

In Fig. 5(b), we represent the power characteristic of the system at the exceptional point calculated with the continuous model. As seen, the results predicted by Eq. (21) overlap precisely with the effective transmission line results. Importantly, even the slightest detuning from the operation at the exceptional point will break the phase synchronization condition and reveal a power beating characteristic. This is shown in Fig. 5(c), where we depict the power gain of the system as a function of the number of transistors when the effective permittivity of line 2 is changed from $\varepsilon_{ef,2} = \varepsilon_{ef,2}^{\text{EP}}$ (black curve) to $\varepsilon_{ef,2} = 1.05\varepsilon_{ef,2}^{\text{EP}}$ (blue curve) and $\varepsilon_{ef,2} = 0.95\varepsilon_{ef,2}^{\text{EP}}$ (green curve). As seen, when the system is not operated at the exceptional point, the oscillations reappear since the interaction between the ordinary and extraordinary waves is not strictly "constructive" for all points of the line. Nevertheless, for all practical purposes, such an effect would go unnoticed since typical distributed amplifiers do not have more than a dozen transistors [54–59]. The robustness of the power gain for small systems is precisely the reason why such amplifiers are considered to be wideband [50–59].

In Fig. 5(d), we depict the calculated power gain when the capacitance C_{gd} is not neglected (we use $C_{gd} = 0.01$ pF [53]) and the frequency of operation is changed from $\omega_0/(2\pi) = 5$ GHz (black solid curve) to $\omega = 3\omega_0$ (green dashed curve) and $\omega = 6\omega_0$ (blue solid curve). As seen, even when the FETs do not behave as ideal isolators and the system is no longer operated at the exceptional point, the system response remains nearly the same as in the ideal scenario for structures with $N_{FET} = 100$, despite the variations in the operation frequency. Indeed, in most practical implementations, the power gain is only limited by dissipation [53] and by the frequency response of the transistors, which for microwave FETs tends to break down around 20 GHz [60].

IV. CONCLUSIONS

We proposed a 1D implementation of the nonreciprocal and non-Hermitian MOSFET-MTM based on transmission lines capacitively coupled through FET isolators. We studied the wave propagation in the system using an effective medium approach. The homogenized system response is non-Hermitian and characterized by a broken time-reversal symmetry. It was shown that the interaction between the waves in the gate and drain lines can lead to regimes wherein the FETs act as gain elements, as well as regimes where they function as dissipative elements. Interestingly, the system parameters can be adjusted so that the structure operates at an exceptional point, where both eigenstates coalesce and degenerate. At the exceptional point, the wave propagation is not described by "Bloch waves" but rather by polynomial-type Bloch waves. In this regime, there are no power oscillations and the wave can continuously draw power from the dc bias. The voltage and the current grow linearly with the propagation distance while the power grows quadratically. Furthermore, we demonstrated that typical distributed amplifiers are operated exactly at the exceptional point.

ACKNOWLEDGMENTS

[1] N. J. Dunford and J. T. Schwartz, *Linear Operators, Parts I and II* (Wiley, Hoboken, New Jersey, 1988).

[2] N. Moiseyev, *Non-Hermitian Quantum Mechanics* (Cambridge University Press, Cambridge, UK, 2011).

[3] V. V. Konotop, J. Yang, and D. A. Zezyulin, Nonlinear waves in PT-symmetric systems, Rev. Mod. Phys. **88**, 035002 (2016).

[4] L. Feng, R. El-Ganainy, and L. Ge, Non-Hermitian photonics based on parity–time symmetry, Nat. Photonics **11**, 752 (2017).

[5] R. El-Ganainy, K. G. Makris, M. Khajavikhan, Z. H. Musslimani, S. Rotter, and D. N. Christodoulides, Non-Hermitian physics and PT symmetry, Nat. Phys. **14**, 11 (2018).

[6] M.-A. Miri and A. Alù, Exceptional points in optics and photonics, Science **363**, eaar7709 (2019).

[7] H. Shen, B. Zhen, and L. Fu, Topological band theory for non-Hermitian Hamiltonians, Phys. Rev. Lett. **120**, 146402 (2018).

[8] H. Shen and L. Fu, Quantum oscillation from in-gap states and a non-Hermitian Landau level problem, Phys. Rev. Lett. **121**, 026403 (2018).

[9] M. Papaj, H. Isobe, and L. Fu, Nodal arc of disordered Dirac fermions and non-Hermitian band theory, Phys. Rev. B **99**, 201107(R) (2019).

[10] Y. Ashida, Z. Gong, and M. Ueda, Non-Hermitian physics, Adv. Phys. **69**, 249 (2020).

[11] K. G. Makris, R. El-Ganainy, D. N. Christodoulides, and Z. H. Musslimani, Beam dynamics in PT symmetric optical lattices, Phys. Rev. Lett. **100**, 103904 (2008).

[12] C. E. Rüter, K. G. Makris, R. El-Ganainy, D. N. Christodoulides, M. Segev, and D. Kip, Observation of parity–time symmetry in optics, Nat. Phys. **6**, 192 (2010).

[13] Z. Lin, J. Schindler, F. M. Ellis, and T. Kottos, Experimental observation of the dual behavior of PT-symmetric scattering, Phys. Rev. A **85**, 050101(R) (2012).

[14] T. Kodera, D. L. Sounas, and C. Caloz, Artificial Faraday rotation using a ring metamaterial structure without static magnetic field, Appl. Phys. Lett. **99**, 031114 (2011).

[15] Z. Wang, Z. Wang, J. Wang, B. Zhang, J. Huangfu, J. D. Joannopoulos, M. Soljacic, and L. Ran, Gyrotropic response in the absence of a bias field, Proc. Natl. Acad. Sci. U. S. A. **109**, 13194 (2012).

[16] T. Kodera, D. L. Sounas, and C. Caloz, Magnetless non-reciprocal metamaterial (MNM) technology: Application to microwave components, IEEE Trans. Microw. Theory Tech. **61**, 1030 (2013).

[17] S. Buddhiraju, A. Song, G. T. Papadakis, and S. Fan, Non-reciprocal metamaterial obeying time-reversal symmetry, Phys. Rev. Lett. **124**, 257403 (2020).

[18] S. Lannebère, D. E. Fernandes, T. A. Morgado, and M. G. Silveirinha, Nonreciprocal and non-Hermitian material response inspired by semiconductor transistors, Phys. Rev. Lett. **128**, 013902 (2022).

[19] T. G. Rappoport, T. A. Morgado, S. Lannebère, and M. G. Silveirinha, Engineering transistor-like optical gain in two-dimensional materials with Berry curvature dipoles, Phys. Rev. Lett. **130,** 076901 (2023).

[20] S. Lannebère, D. E. Fernandes, T. A. Morgado, and M. G. Silveirinha, Chiral-gain photonics, arXiv:2405.15606.

[21] T. Kato, *Perturbation Theory for Linear Operators, Die Grundlehren der mathematischen Wissenschaften, Band 132* (Springer-Verlag, New York, 1966).

[22] M. V. Berry, Physics of nonhermitian degeneracies, Czech. J. Phys. **54,** 1039 (2004).

[23] W. D. Heiss, The physics of exceptional points, J. Phys. A **45,** 444016 (2012).

[24] J. Wiersig, Enhancing the sensitivity of frequency and energy splitting detection by using exceptional points: Application to microcavity sensors for single-particle detection, Phys. Rev. Lett. **112,** 203901 (2014).

[25] Z.-P. Liu, J. Zhang, S. K. Özdemir, B. Peng, H. Jing, X.-Y. Lü, C.-W. Li, L. Yang, F. Nori, and Y.-x. Liu, Metrology with PT-symmetric cavities: Enhanced sensitivity near the PT-phase transition, Phys. Rev. Lett. **117,** 110802 (2016).

[26] H. Hodaei, A. U. Hassan, S. Wittek, H. Garcia-Gracia, R. El-Ganainy, D. N. Christodoulides, and M. Khajavikhan, Enhanced sensitivity at higher-order exceptional points, Nature **548,** 187 (2017).

[27] W. Chen, ŞK Özdemir, G. Zhao, J. Wiersig, and L. Yang, Exceptional points enhance sensing in an optical microcavity, Nature **548,** 192 (2017).

[28] H.-K. Lau and A. A. Clerk, Fundamental limits and non-reciprocal approaches in non-Hermitian quantum sensing, Nat. Commun. **9,** 4320 (2018).

[29] M. Zhang, W. Sweeney, C. W. Hsu, L. Yang, A. D. Stone, and L. Jiang, Quantum noise theory of exceptional point amplifying sensors, Phys. Rev. Lett. **123,** 180501 (2019).

[30] C. Dembowski, H.-D. Gräf, H. L. Harney, A. Heine, W. D. Heiss, H. Rehfeld, and A. Richter, Experimental observation of the topological structure of exceptional points, Phys. Rev. Lett. **86,** 787 (2001).

[31] T. Gao, E. Estrecho, K. Y. Bliokh, T. C. H. Liew, M. D. Fraser, S. Brodbeck, M. Kemp, C. Schneider, S. Höfling, Y. Yamamoto, F. Nori, Y. S. Kivshar, A. G. Truscott, R. G. Dall, and E. A. Ostrovskaya, Observation of non-Hermitian degeneracies in a chaotic exciton-polariton billiard, Nature **526,** 554 (2015).

[32] J. Doppler, A. A. Mailybaev, J. Böhm, U. Kuhl, A. Girschik, F. Libisch, T. J. Milburn, P. Rabl, N. Moiseyev, and S. Rotter, Dynamically encircling an exceptional point for asymmetric mode switching, Nature **537,** 76 (2016).

[33] H. Xu, D. Mason, L. Jiang, and J. G. E. Harris, Topological energy transfer in an optomechanical system with exceptional points, Nature **537,** 80 (2016).

[34] J. W. Yoon, Y. Choi, C. Hahn, G. Kim, S. H. Song, K.-Y. Yang, J. Y. Lee, Y. Kim, C. S. Lee, J. K. Shin, H.-S. Lee, and P. Berini, Time-asymmetric loop around an exceptional point over the full optical communications band, Nature **562,** 86 (2018).

[35] K. Kawabata, T. Bessho, and M. Sato, Classification of exceptional points and non-Hermitian topological semimetals, Phys. Rev. Lett. **123,** 066405 (2019).

[36] E. J. Bergholtz, J. C. Budich, and F. K. Kunst, Exceptional topology of non-Hermitian systems, Rev. Mod. Phys. **93,** 015005 (2021).

[37] Z. Lin, H. Ramezani, T. Eichelkraut, T. Kottos, H. Cao, and D. N. Christodoulides, Unidirectional invisibility induced by PT-symmetric periodic structures, Phys. Rev. Lett. **106,** 213901 (2011).

[38] A. Regensburger, C. Bersch, M.-A. Miri, G. Onishchukov, D. N. Christodoulides, and U. Peschel, Parity–time synthetic photonic lattices, Nature **488,** 167 (2012).

[39] L. Feng, Y.-L. Xu, W. S. Fegadolli, M.-H. Lu, J. E. B. Oliveira, V. R. Almeida, Y.-F. Chen, and A. Scherer, Experimental demonstration of a unidirectional reflectionless parity-time metamaterial at optical frequencies, Nat. Mater. **12,** 108 (2013).

[40] B. Peng, ŞK Özdemir, F. Lei, F. Monifi, M. Gianfreda, G. L. Long, S. Fan, F. Nori, C. M. Bender, and L. Yang, Parity–time-symmetric whispering-gallery microcavities, Nat. Phys. **10,** 394 (2014).

[41] H. Zhou, C. Peng, Y. Yoon, C. W. Hsu, K. A. Nelson, L. Fu, J. D. Joannopoulos, M. Soljačić, and B. Zhen, Observation of bulk Fermi arc and polarization half charge from paired exceptional points, Science **359,** 1009 (2018).

[42] T. E. Lee and C.-K. Chan, Heralded magnetism in non-Hermitian atomic systems, Phys. Rev. X **4,** 041001 (2014).

[43] K. Kawabata, Y. Ashida, and M. Ueda, Information retrieval and criticality in parity-time-symmetric Systems, Phys. Rev. Lett. **119,** 190401 (2017).

[44] M. Nakagawa, N. Kawakami, and M. Ueda, Non-Hermitian Kondo effect in ultracold alkaline-earth atoms, Phys. Rev. Lett. **121,** 203001 (2018).

[45] J. Li, A. K. Harter, J. Liu, L. de Melo, Y. N. Joglekar, and L. Luo, Observation of parity-time symmetry breaking transitions in a dissipative Floquet system of ultracold atoms, Nat. Commun. **10,** 855 (2019).

[46] B. Dóra, M. Heyl, and R. Moessner, The Kibble-Zurek mechanism at exceptional points, Nat. Commun. **10,** 2254 (2019).

[47] Y. Wu, W. Liu, J. Geng, X. Song, X. Ye, C.-K. Duan, X. Rong, and J. Du, Observation of parity-time symmetry breaking in a single-spin system, Science **364,** 878 (2019).

[48] L. Xiao, K. Wang, X. Zhan, Z. Bian, K. Kawabata, M. Ueda, W. Yi, and P. Xue, Observation of critical phenomena in parity-time-symmetric quantum dynamics, Phys. Rev. Lett. **123,** 230401 (2019).

[49] W. D. Heiss, Exceptional points of non-Hermitian operators, J. Phys. Math. Gen. **37,** 2455 (2004).

[50] E. L. Ginzton, W. R. Hewlett, J. H. Jasberg, and J. D. Noe, Distributed amplification, Proc. IRE **36,** 956 (1948).

[51] J. Beyer, S. N. Prasad, R. Becker, J. E. Nordman, and G. K. Hohenwarter, MESFET distributed amplifier design guidelines, IEEE Trans. Microw. Theory Tech. **32,** 268 (1984).

[52] R. Pengelly, S. M. Wood, J. W. Milligan, S. T. Sheppard, and W. L. Pribble, A review of GaN on SiC high electron-mobility power transistors and MMICs, IEEE Trans. Microw. Theory Tech. **60,** 1764 (2012).

[53] D. M. Pozar, *Microwave Engineering*, 4th ed. (Wiley, Hoboken, 2012).

[54] B. M. Green, V. Tilak, S. Lee, H. Kim, J. A. Smart, K. J. Webb, J. R. Shealy, and L. F. Eastman, High-power broadband AlGaN/GaN HEMT MMICs on SiC substrates, IEEE Trans. Microw. Theory Tech. **49**, 2486 (2001).

[55] D. E. Meharry, R. J. Lender, K. Chu, L. L. Gunter, and K. E. Beech, in *IEEE MTT-S Int. Microw. Symp. Dig.* (2007), pp. 631.

[56] J. Gassmann, P. Watson, L. Kehias, and G. Henry, in *IEEE MTT-S Int. Microw. Symp. Dig.* (2007), pp. 615.

[57] C. Campbell, C. Lee, V. Williams, M. Y. Kao, H. Q. Tserng, and P. Saunier, in *IEEE Compound Semicond. Integr. Circuits Symp.* (2008), pp. 1.

[58] K. W. Kobayshi, Y. C. Chen, I. Smorchkova, B. Heying, W. B. Luo, W. Sutton, M. Wojtowicz, and A. Oki, in *IEEE RFIC Symp.* (2009), pp. 369.

[59] K. A. Grebennikov, N. Kumar, and B. S. Yarman, *Broadband RF and microwave amplifiers* (CRC Press, Boca Raton, 2015).

[60] MWT-INC Product Selection Guide, https://www.mwtinc.com/wp-content/uploads/2017/03/Selection_Guide_2020-2021_web.pdf